J Sol-Gel Sci Technol (2009) 49:112–124
DOI 10.1007/s10971-008-1845-6

ORIGINAL PAPER

One-step preparation of thiol-modified mesoporous silica spheres with various functionalization levels and different pore structures

Fabrice O. M. Gaslain · Cyril Delacôte · Alain Walcarius · Bénédicte Lebeau

Received: 18 July 2008 / Accepted: 14 October 2008 / Published online: 4 November 2008

Abstract A wide range of mercaptopropyl-functionalized silica spherical particles of MCM-41 and MCM-48 (M41S family) have been prepared by co-condensation of mercaptopropyl trimethoxysilane (MPTMS) or mercaptopropyl triethoxysilane (MPTES) and tetraethoxysilane (TEOS) precursors in hydroalcoholic medium in the presence of a cationic surfactant as templating agent and ammonia as catalyst. It was possible to control the mesostructure type (hexagonal or cubic) by monitoring the water-to-ethanol ratio and the type of organoalkoxysilane precursor employed. Materials displaying various functionalization levels were obtained by varying the MPTMS or MPTES contents from 3 to 50% in the co-condensation synthesis medium. This gave rise to a wide range of porous solids with approximately the same particle size and morphology but featuring different functionalization levels and various degrees of structural order. They were characterized by X-ray diffraction (XRD), N_2 adsorption-desorption isotherms and BET analysis, scanning and transmission electron microscopy, ^{29}Si and ^{13}C solid state nuclear magnetic resonance (NMR), particle size distribution measurements, and elemental chemical analysis. Mercaptopropyl groups were readily incorporated with high yields (>90%) by the co-condensation route. All samples exhibited spherical morphology with similar particle size but both the level of ordering and porosity of solids obtained by co-condensation were found to decrease when increasing the amount of organo-functional groups.

Keywords Mesoporous silica · MCM-41 · MCM-48 · Mercaptopropyl · Direct functionalization

1 Introduction

Among the most recent solutions investigated for the elaboration of adsorbent materials for heavy metal remediation, silica based organic-inorganic ordered mesoporous materials have received an increasing interest. These mesostructured silica discovered in the 1990s [1, 2] synthesised in the presence of surfactant as a structure-directing agent materials are characterized by high surface areas, uniform and controlled pores sizes, and a long-range order. Unlike zeolites, the pore size of mesoporous silica is large enough to accommodate a variety of large molecules, and the high density of silanol groups on the pore walls is beneficial to the introduction of functional groups with high coverage [3]. In fact, several kinds of surface modification have been conducted for providing new functions to the surfaces [4–12]. Surface modifications have been generally achieved by direct co-condensation and post-synthesis grafting methods with organoalkoxysilanes, and many of these efforts have been summarized in numerous recent reviews [13–17]. In short, those materials take advantage of both the inorganic framework (non-swelling and stable under acidic conditions, which can be prepared with desired porosity and high surface area) and the complexation capacity of the organic functional groups anchored onto the silica surfaces [18].

F. O. M. Gaslain · B. Lebeau (✉)
Laboratoire de Matériaux à Porosité Contrôlée, Ecole Nationale Supérieure de Chimie de Mulhouse, Université de Haute Alsace, CNRS UMR 7016, 3 rue Alfred Werner, 68093 Mulhouse, France
e-mail: benedicte.lebeau@uha.fr

C. Delacôte · A. Walcarius
Laboratoire de Chimie Physique et Microbiologie pour l'Environnement - Université H. Poincaré Nancy I, CNRS UMR 756, 405 rue de Vandoeuvre, 54600 Villers-les-Nancy, France

Functionalised mesoporous silicas with a high density of amino groups *via* direct co-condensation and post-synthesis grafting methods and well-defined mesochannels that can enhance the accessibilities of molecules have been applied to solid-base adsorbents for toxic metal cations, such as cobalt, copper, zinc and lead [19–27]. Different strategies to improve the affinity and selectivity of these materials have been applied by either selecting the most adequate framework system with high performance ligands [28] or by increasing the density of functional groups while retaining the open space [29–33]. From these abundant and interesting screenings, the scientific knowledge has been drastically improved.

Among the rich variety of ligands available: the mercaptopropyl group has attracted a lot of attention due to its wide availability and high capacity to fix Hg(II) as reported by the groups of Liu, Mercier, and Pinnavaia [29, 30, 34–44]. Hence, mercaptopropyl ligands and their post-synthesis grafting onto mesoporous silica for metal remediation have been very well investigated. Other applications have also emerged from these advances: (1) mercaptopropyl-grafted silica (MPS) have been used to immobilise enzymes [45] or proteins [46], (2) MPS have been employed as supports for metal nanoparticles [47] and in the formation of nanowires [48, 49], (3) and sulfonic acid-functionalised mesoporous silica ion exchangers with large inner surface have been developed by in situ oxidisation of the mercaptopropyl group [50–55].

Coming back to sorbent applications, the efficiency of a functionalised material is usually assessed by its capacity to retain pollutants. However, only few studies looked into the accessibility of pollutant species to the active sites [56] and mass-transfer reaction behaviours for these systems [26, 29–33, 57–68]; but their results were impossible to compare. For a possible comparison, it is necessary to make similar materials in terms of ligands, particle size and shape; but with different porous networks and loadings to do a comparative evaluation of mass-transfer rates. A spherical morphology would be helpful since it is preferable to optimize accessibility to the particle heart for unidimensional porous system such as MCM-41 type solids, it is probably the easiest to obtain and moreover a diffusion model well-adapted for spherical particle has proven its efficiency to describe mass transfers within mesoporous siliceous sorbents for heavy metals [67]. Here, we present the synthetic ways to make very similar M41S materials functionalised by mercaptopropyl groups using a direct co-condensation route with their complete characterisation. The mercaptopropyl ligand has been chosen over many other ligands, not for its relative efficiency as a Hg(II) sorbent; but as a model ligand since it benefits from a very extensive literature. Special care has been made to synthesise all the materials in very similar conditions in order to have similar spherical particle sizes and frameworks (equivalent silanol types with the same functionalization process): the main difference lying in the porous network geometry (MCM-41 and MCM-48). The aim of this work is to draw trends for these types of materials.

2 Experimental

2.1 Chemicals and reagents

All reagents were of analytical grade and were used as received from the suppliers: tetraethoxysilane (TEOS, >98%, Aldrich), mercaptopropyltrimethoxysilane (MPTMS, 95%, Lancaster), mercaptopropyltriethoxysilane (MPTES, 95%, Lancaster), cetyltrimethylammonium bromide (CTMABr, 98%, Fluka), ammonia solution (33% aqueous, Riedel de Haën), ethanol (95%, Riedel de Haën) and hydrochloric acid (HCl, 37%, Riedel de Haën). All the distilled water needed for experiments was provided from a commercial bench top distillation apparatus.

2.2 Preliminary study

One important aspect of this work was to produce mesoporous silica particles of different framework geometries and various mercaptopropyl loadings; but of spherical shape and relative particle size homogeneity. A preliminary study was thus necessary to optimise the different experimental protocols. Although the synthesis of mesoporous spherical particles of MCM-41 with a satisfactorily narrow pore-size distribution and regular hexagonal pore structure was already known and the procedure was previously published [59, 69], the synthesis of MCM-48 prepared in similar conditions was not available from the literature.

From the 1990s, it has been well known that the presence of alcohol can disrupt the formation of liquid-crystal phases in CTMA-containing solutions [70]. Scientists from Mobil Research and Development Corp. also found during this period that ethanol can disrupt the most stable hexagonal liquid-crystal phase [71] to form lamellar or cubic liquid-crystal phases. According to this liquid-crystal templating (LCT) mechanism argumentation proposed by these workers [72], varying the water to ethanol ratio would probably provoke modifications of the surfactant liquid-crystal phase. Having this consideration in mind and already using a water-ethanol system for the synthesis of MCM-41 materials [59, 66–68], the amount of water was modified in such a manner to obtain MCM-48 materials. Using similar synthetic protocols, it was found that a mixture of 50/50 vol.% water/ethanol would result in the

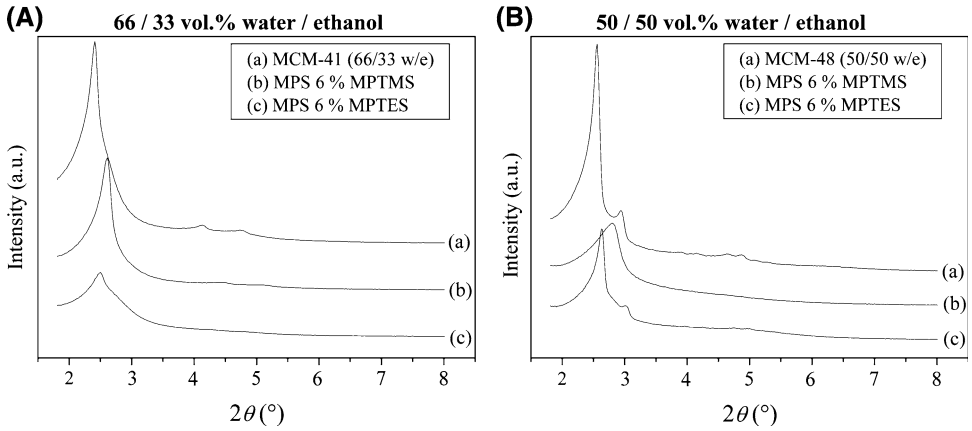

Fig. 1 XRD patterns of materials prepared with (**a**) 66/33 and (**b**) 50/50 vol.% water/ethanol

formation of MCM-41 materials (Fig. 1a, curve a); whereas a mixture of 66/33 vol.% water/ethanol would result in the formation of MCM-48 materials (Fig. 1b, curve a). In both cases, the particles were of spherical shape with relative particle size homogeneity within the same range.

With both raw M41S materials synthesised successfully, the following step was to graft them with mercaptopropyl groups using a direct functionalising process. Here, the main difficulty consisted of keeping particles with similar size and morphology since these ligands can introduce particle shape modifications [73]. Two functionalization precursors (i.e.: MPTMS and MPTES) were apprehended to graft the silica matrices. The choice for one or another precursor has been motivated by studying which precursor would be most suited for the type of framework topology considered: hexagonal MCM-41 or cubic MCM-48 mesostrutures. The study consisted of preparing materials using similar protocols that led to the formation of MCM-41 and MCM-48 materials but replacing part of the TEOS by 6 mol% of either MPTMS or MPTES functionalising groups in the starting sol (see method described in Sect. 2.3). After extraction and drying all resulting materials, they have been characterised by XRD measurements and their patterns have been compared to those of non-grafted calcined MCM-41 and MCM-48 (Fig. 1). With a 50/50 vol.% water/ethanol mixture, the hexagonal geometry was best retained when using MPTMS functionalising groups. Using MPTES as a functionalization group reduced the porous mesostructure order (Fig. 1b, curves b–c). However; in the case of a 66/33 vol.% water/ethanol mixture was employed, the opposite scenario could be observed, in other words, the cubic mesostructure geometry was only retained when using MPTES as a functionalising group and not with MPTMS (Fig. 1a, curves b–c).

The type of solvent generated during the condensation of each functionalising group (i.e.: ethanol for MPTES and methanol for MPTMS) is most probably the predominant factor to obtain a mercaptopropylsilyl-functionalized mesoporous material of either MCM-41 or MCM-48 geometry. Consequently, one party could have argued that since the functionalized MCM-41 material was best synthesised with MPTMS, it could have been more judicious to substitute ethanol by methanol and TEOS by TMOS to favour the hexagonal micellar phase [70, 74]. Another possibility that is well documented in the literature would have been to add various counterions in order to influence on the formation of one phase to another. However, all these changes, although conceivable, could have induced further modifications in the final materials, in terms of particle size and morphology, pore size or silica condensation degree, and our comparative approach would not have possible with these experimental conditions.

2.3 Preparation of thiol-functionalized hybrid materials by direct synthesis

Organically modified mesoporous silica spheres with relative particle size homogeneity were prepared following the one-pot synthesis route. In this study, samples with the MCM-41 (hexagonal) or MCM-48 (cubic) mesoporous architectures containing variable concentrations of mercaptopropyl groups have been prepared.

The typical molar composition of reagents for mesostructured silicas with the MCM-41 architecture was 1 SiO_2 precursor: 0.41 CTMABr: 14.5 ammonia: 53 ethanol: 180 water (SiO_2 precursors being mixtures of MPTMS and TEOS with ratios varying from 0 to 50% MPTMS: TEOS). First, 2.4 g of CTMABr were dissolved in 50 mL of distilled water and 45 mL of ethanol under stirring. After complete dissolution of the surfactant, 13 mL of ammonia solution were added. In the mean time, a precursor solution was prepared by dissolving appropriate ratios of MPTMS and TEOS in 5 mL of ethanol, which was then added to the surfactant-plus-catalyst solution under vigorous stirring. Condensation occurred within about 2 min and the resulting white precipitate was stirred for a remaining 2 h at room temperature. The product was then isolated by

vacuum filtration on a Büchner funnel and washed alternatively with water and ethanol. The resulting powder was dried under vacuum ($<10^{-2}$ bar) for 24 h at 60 °C. The surfactant was then removed from the hybrid material by acid/solvent extraction by suspending the solid particles in 1 mol L^{-1} HCl in ethanol (1 g of solid powder in 100 mL of solution), which was then allowed to reflux for 24 h [75]. Finally, solid products were recovered by filtration, washed with ethanol and dried according to the aforementioned conditions. Functionalized MCM-41 materials have been named herein as $MPS_{(HEX)}$ (mercaptopropyl-silica with hexagonal mesoporous geometry), followed by the molar MPTMS proportion relative to TEOS found in the starting sols: MCM-41 or MPS_{HEX}-0%, MPS_{HEX}-3%, MPS_{HEX}-6%, MPS_{HEX}-9%, MPS_{HEX}-12%, MPS_{HEX}-15%, MPS_{HEX}-20%, MPS_{HEX}-25%, MPS_{HEX}-30%, MPS_{HEX}-40% and finally MPS_{HEX}-50%.

A similar procedure to the one just described above was employed for the syntheses of MCM-48 porous silicas. Only the amount of water was doubled compared to the water quantity used in the preparation of MCM-41 materials and MPTMS was replaced by MPTES using the same MPTES: TEOS ratios. Comparatively to the precedent series, the resulting functionalized MCM-48 materials have been named herein as $MPS_{(CUB)}$ (mercaptopropyl-silica with cubic mesoporous geometry), followed by the molar MPTES proportion relative to TEOS found in the starting sols: MCM-48 or MPS_{CUB}-0%, MPS_{CUB}-3%, MPS_{CUB}-6%, MPS_{CUB}-9%, MPS_{CUB}-12%, MPS_{CUB}-15%, MPS_{CUB}-20%, MPS_{CUB}-25%, MPS_{CUB}-30%, MPS_{CUB}-40% and MPS_{CUB}-50%.

2.4 Instrumentation

The materials were characterised by various physico-chemical techniques. Powder X-ray diffraction patterns were recorded at room temperature on a powder PANanalytical X'PERT PRO diffractometer, equipped with a Cu anode (quartz monochromator, Kα radiation, $\lambda = 0.15406$ nm, scanning range, 0.5–10°(2θ), step size: 0.02° per 2s). Nitrogen adsorption-desorption measurements were performed at 77 K with a Coulter instrument (model SA 3100) or a Micromeritics instrument (model Tristar), in the relative pressure range from about in the relative pressure (P/P_O) range from about 10^{-5} to 0.99. All samples were dried and outgassed at 90 °C for a minimum of 12 h under vacuum before carrying out the nitrogen adsorption experiments. BET specific surface areas were calculated from adsorption isotherms in the relative pressure range from 0.05 to 0.20. The single-point total pore volumes were estimated from the amount of nitrogen adsorbed at a relative pressure of approximately 0.98. Pore size distributions were calculated from the desorption branch of isotherms by using the BJH (Barrett, Joyner and Halenda) approach modified by the KJS (Kruck, Jaroniec and Sayari) method. Scanning electron microscopy (SEM) pictures were obtained from a PANanalytical XL30 FEG apparatus operating at 5 KeV. Prior to SEM observations, samples were coated with gold (thickness ~20 nm) using a cathodic sputtering device. Transmission electron microscopy (TEM) pictures were obtained from a Philips CM30 microscope operating at 200 keV. Samples were dispersed in ethanol before being deposited on a copper grid covered with carbon film. Particle size distribution was measured using a light scattering analyser instrument from Horiba (model LA920), based on the Mie scattering theory. ^{13}C and ^{29}Si solid state nuclear magnetic resonance (MAS NMR) experiments were performed on a Bruker Avance II 300 MHz apparatus ($B_0 = 7.1$ T) on a standard double bearing 7 mm broad band probe rotating at a spinning frequency of 4 kHz. ^{29}Si MAS with proton decoupling experiments were run with a pulse of 1.7 µs ($\pi/6$) and a recycling delay of 80 s. Cross-polarization coupled with MAS technique was used for ^{13}C NMR experiments with a pulse of 4.7 µs ($\pi/2$), a contact time of 2 ms and a recycle delay of 6 s. The average number of scans was about 1000 for all samples and whatever the NMR experiment. Elemental analyses of C, H, N and S elements of the final materials were performed at the Service Central d'Analyse of the CNRS in Lyon, France, in order to determine the amount of organic moieties.

3 Results and discussion

3.1 Textural and structural characterisation

The M41S mercaptopropylsilyl-functionalized mesoporous silica materials have been prepared through a direct assembly pathway at room temperature in the presence of a surfactant template (CTMABr) in conditions leading to the formation of regular spheres with internal mesostructure (ammonia catalyst in water/ethanol medium). As it has been mentioned several times, one important aspect of this work was to produce mesoporous silica particles of different framework geometries and various mercaptopropyl loadings; but of spherical shape and relative particle size homogeneity. This morphology was checked by SEM picture analyses (Fig. 2) and by studying the particle size distribution (Table 1). Consistent with previous reports using similar synthetic conditions [66–68], SEM pictures revealed that all materials had spherical morphologies with a broad size distribution varying from 100 to 1000 nm. However, those particles tend to agglomerate in large chucks of 5–15 µm. Also the individual particle size remained approximately constant (except for cubic

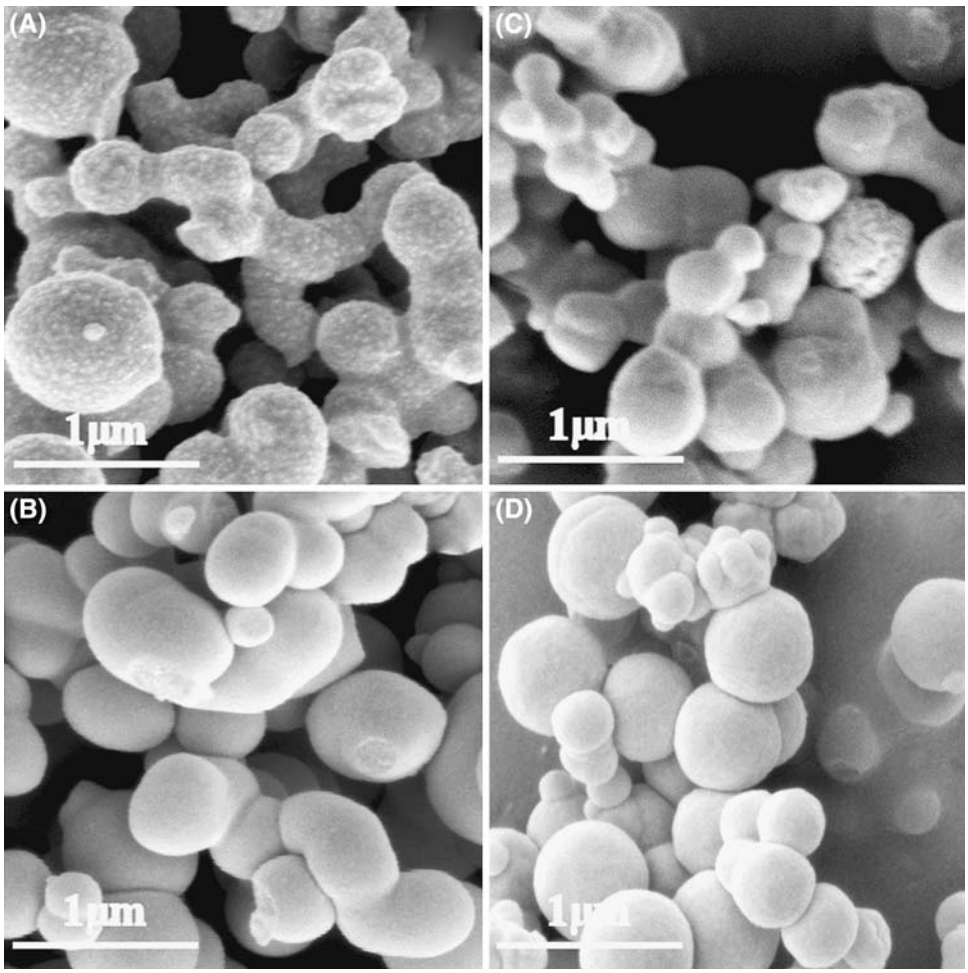

Fig. 2 SEM pictures of MPS_{HEX} (**a**, **b**) and MPS_{CUB} (**c**, **d**) materials obtained by direct synthesis: pure silica (**a**, **c**) and 9% mercaptopropyl functionalised solids (**b**, **d**)

materials loaded with more than 25% MPTES), the aggregate size were significantly larger for materials containing a large fraction of mercaptopropyl functions. This can be ascribed to increased hydrophobicity of these hybrids in comparison to none or low functionalised materials favouring the agglomeration in relatively aqueous media.

Figure 3 depicts the XRD patterns of mesoporous silicas of MCM-41 (A) and MCM-48 (B) types functionalised with different molar ratio of MPTMS and MPTES, respectively. Several categories can be distinguished in the hexagonal series (i.e. MPS_{HEX}). The pure material and low MPTMS loaded materials (3% up to 12%) show XRD patterns (Fig. 3a, curves a–e) characteristic of well ordered hexagonal pore arrangements with diffraction peaks that can be assigned to (100), (110) and (200) reflections in a *P*6 *mm* hexagonal symmetry. In these cases, the sharp diffraction peaks are gradually shifted to higher 2θ angles and their intensities start to diminish indicating a lattice shrinkage together with a loss of pore ordering. For this range of materials, the hexagonal structure was further evidenced by TEM images presented in our previous work [52]. When the MPTMS loading was further increased (15% to 50%), the single low-angle XRD peak started to considerably broaden up to a point where hardly any diffraction could be detectable (Fig. 3a, curves f–k). This feature is characteristic of materials with a mesoporous wormhole framework structure, such as materials of the MSU series synthesised in a neutral route [76].

In the cubic series (i.e. MPS_{CUB}), the pure material shows a XRD pattern with sharp peaks characteristic of well ordered cubic pore arrangement (Fig. 3b, curve a). The eight XRD reflection peaks (211), (220), (321), (400), (420), (332), (422) and (431) can be indexed in a *Ia*3*d* cubic structure. TEM images also give evidence of the cubic structure (Fig. 4a). At low loadings of mercaptopropyl groups (3% up to 12%), the XRD patterns were also characteristic of ordered cubic pore arrangement and very similar to each other (no 2θ shifts), thus for these materials, the lattice parameters remained very similar. Only the *d* spacing decreased slightly compared to the pure silica material. This observation is completed by looking at TEM images: with 6% MPTES loading, the material mesoporosity with a cubic arrangement is easily visible even if the

Table 1 Physical characteristics

Sample name	N_2 ads./des.			Particle size	
	Surface area[a] (m^2 g^{-1} STP)	Pore volume[a] (mL g^{-1} STP)	Pore size[a] (Å)	Isolated particles[b] (μm)	Aggregates[b] (μm)
MCM-41	884	0.68	31.4	n/m*	n/m*
MPS $_{HEX}$-3%	1368	0.89	29.1	0.51 ± 0.24	2.83 ± 3.98
MPS $_{HEX}$-6%	1538	0.84	28.0	0.39 ± 0.20	2.87 ± 2.69
MPS $_{HEX}$-9%	1713	0.75	26.9	0.45 ± 0.20	2.86 ± 1.48
MPS_{HEX}-12%	1615	0.72	26.6	0.39 ± 0.19	3.87 ± 1.94
MPS_{HEX}-15%	1465	0.66	26.9	0.39 ± 0.18	4.62 ± 2.53
MPS_{HEX}-20%	1162	0.56	27.4	0.39 ± 0.16	5.50 ± 2.96
MPS_{HEX}-25%	843	0.43	28.7	0.30 ± 0.14	6.54 ± 3.24
MPS_{HEX}-30%	760	0.39	n/m**	0.34 ± 0.14	7.63 ± 4.05
MPS_{HEX}-40%	546	0.28	n/m**	0.26 ± 0.13	12.56 ± 6.95
MPS_{HEX}-50%	353	0.18	n/m**	<0.26	12.72 ± 8.29
MCM-48	986	0.80	31.9	n/m*	n/m*
MPS $_{CUB}$-3%	1193	0.83	30.4	0.39 ± 0.17	3.15 ± 1.88
MPS $_{CUB}$-6%	1079	0.73	29.9	0.39 ± 0.19	2.07 ± 1.38
MPS $_{CUB}$-9%	966	0.58	29.0	0.39 ± 0.17	3.58 ± 1.93
MPS_{CUB}-12%	946	0.52	28.2	0.39 ± 0.16	4.59 ± 2.43
MPS_{CUB}-15%	860	0.47	28.1	0.34 ± 0.16	5.31 ± 2.83
MPS_{CUB}-20%	691	0.37	28.5	0.34 ± 0.16	5.80 ± 3.57
MPS_{CUB}-25%	607	0.32	27.6	0.34 ± 0.15	5.63 ± 2.82
MPS_{CUB}-30%	584	0.30	n/m**	5.12 ± 3.25	9.76 ± 4.49
MPS_{CUB}-40%	488	0.25	n/m**	7.70 ± 3.25	10.64 ± 4.32
MPS_{CUB}-50%	322	0.17	n/m**	10.10 ± 3.50	12.30 ± 5.70

n/m = not measured

[a] Errors on N2-sorption data are estimated to be about 1%

[b] Errors on mean size were calculated from the half width at the half height of the size distribution

* The particle size of non-grafted material was only evaluated by MEB observations. Results were comparable

** BJH method gave aberrant results since the distribution was too large and the pore volume too low

pores are smaller than in the case of a pure material (Fig. 4b). Slowly increasing the loading to 12% MPTES and the visible mesoporosity was considerably reduced even though the ordering was retained (Fig. 4c), which is a clear indication of structural disordering. Increasing further the MPTES loading (15% and 20%) caused a rapid loss of XRD peak and TEM images of MPS_{CUB}-20% (Fig. 4d) were typical of a disordered material. As it could be anticipitated, disordered solids were formed with higher amount of MPTES (25% up to 50%) in the starting sol since all their XRD patterns were flat. At this stage of the study it is difficult to affirm if the XRD data indicate a sudden transition from ordered to disordered solid or the coexistence of both ordered and disordered domain. The TEM observation of the cubic arrangement for the MPS_{CUB}-12% sample (Fig. 4c) seems to favour the first hypothesis. However, if an ordered domain is at the surface (shell) and a disordered one in the core of the particle, a similar TEM observation could be obtained. In this case, the material would present a heterogeneous mesostructure that could result in heterogeneous repartition of thiol functions. Diffusion of species within the porosity would be more complex and adsorption experiments would be more difficult to interprete. TEM analyzes on microtomed sample would help to discern the true hypothesis.

In general, these M41S materials give similar results to those previously reported with materials synthesised in similar systems with both *d*-spacing and pore volume decreasing as the degree of functionalising groups in the reaction mixture is increased [77–81]. Based on Lim et al. hypothesis [77], for MPS modified materials, the silicate-surfactant electrostatic interactions diminish when the number of functional groups increases due to charge compensations arising from the negatively charged thiol function in basic medium. This leads to contraction of the cylindrical micelle size in M41S with higher concentrations of organic surface groups. The authors also suggested an alternate explanation, which would invoke stronger

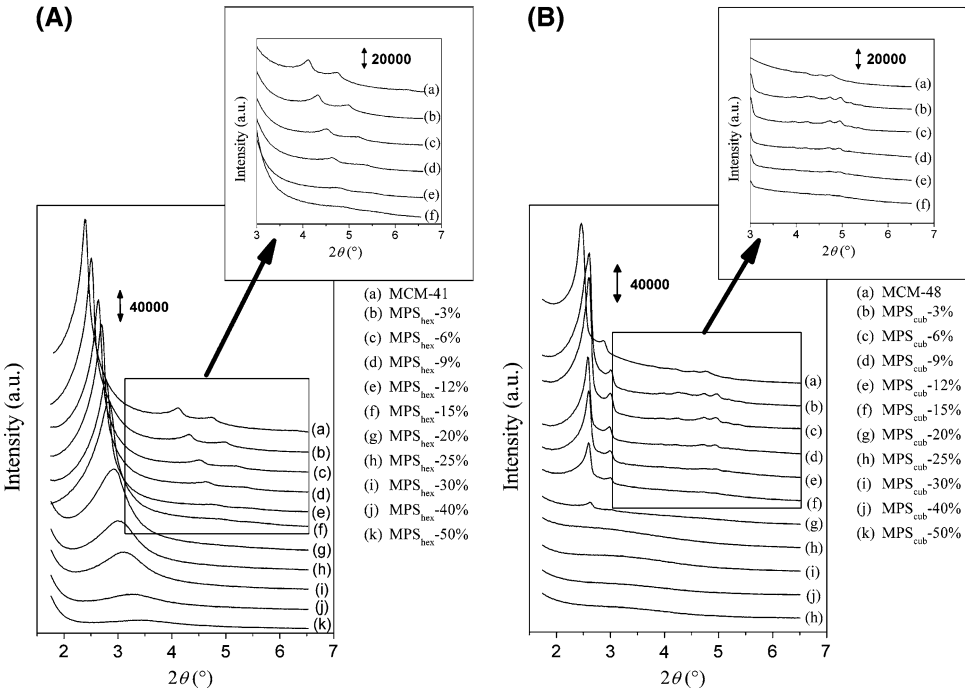

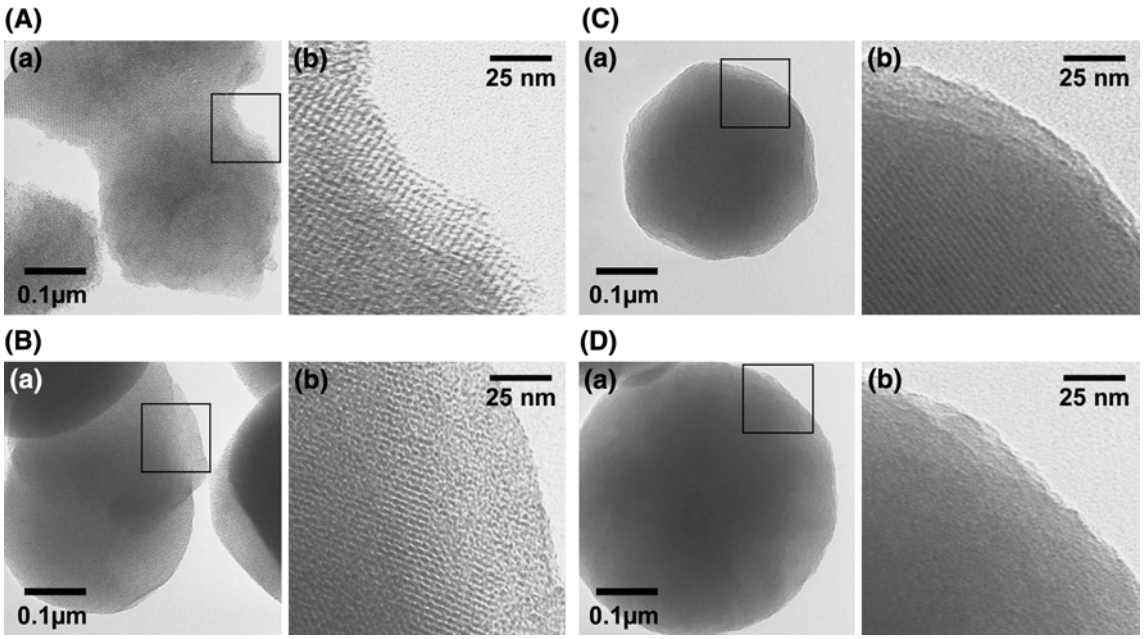

Fig. 3 XRD patterns of (**a**) MPS_{HEX} and (**b**) MPS_{CUB} series

Fig. 4 TEM pictures of (**a**) MCM-48, (**b**) MPS_{CUB}-6%, (**c**) MPS_{CUB}-12% and (**D**) MPS_{CUB}-20%

hydrophobic interactions between the functional groups and the surfactant tails. Such interactions would draw the organic precursors further into the micelles, leading to shrinkage of the pores. The location of the mercaptopropyl functions close to the surfactant tails has been recently shown experimentally in a work on spray-dried mesoporous sheres [82]. However, this observation is in contradiction with the behaviour of materials synthesised with amino-organoalkoxysilanes, since the presence of hydrophilic amino groups counter affect the electrostatic effect and tend to move away from the micelle centre [27].

It is also interesting to notice that they are important differences in framework trends between the MPS modified MCM-41 and MCM-48 structure types. For the MPS_{HEX} series of materials, increasing the mercaptoprpyl loading will gradually modify the ordered hexagonal porous system to a vermicular network before complete disordering; whereas for the MPS_{CUB} series, there is no transitional

phase and the ordered cubic porous network directly give place to completely disordered materials. Although there are framework differences, systematic analyses of sulphur elements for these series of materials revealed a good correlation between the initial percentage of thiol precursors in the starting sols and the final mercaptopropyl loadings (Table 2). This indicates a yield of the synthesis about 100%. However, the carbon and hydrogen compositions are times higher than the calculated theoretical values. This observation is especially true for low MPS functionalised materials.

3.2 Pore size trends

N_2 adsorption-desorption isotherms and pore size distributions obtained by BJH-KJS models for the MPS_{HEX} and MPS_{CUB} series are displayed in Figs. 5 and 6, respectively. Only for the relatively low MPS loaded samples (i.e.: MPS content below 20% in the starting sol), the isotherms are of type IV [83] according to the IUPAC classification [84]. In those cases and for both framework systems, the isotherms exhibit small hysteresis at P/P_O below 0.45, characteristics of capillary condensation of framework-confined mesopores. The inflection position shifted slightly toward lower relative pressures and the volume of nitrogen adsorbed decreased with increased degree of functionalization. However, the more the material was loaded with mercaptopropyl functions, the less important was the hysteresis loop, with isotherms gradually changing from type IV to I. This phenomenon may result from the instability of liquid nitrogen meniscus inside the narrow channels [85, 86]. Nitrogen adsorption measurements of MPS materials obtained from fractions of organosilane larger than 20% exhibited type I isotherms, typical for microporous materials [78].

The specific surface areas calculated by the BET method, the total pore volumes and pore sizes obtained by BJH-KJS models are summarised in Table 1 and represented in Figs. 7 and 8. The first impression we have from those nitrogen adsorption experiments is that they are important differences between the two types of framework systems studied in this paper. The pore size trends (Fig. 6) totally differ from each other: (1) for the hexagonal system, the pore size diminishes proportionally (from ~33 Å to less than 22 Å) with respect to the mercaptopropyl loading rise and the pore volume slowly decreases; 2) for the cubic system, the pore size rather tends to stay constant (~29 Å) with respect to the mercaptopropyl loading rise; but the pore volume rapidly decreases. These results are to be directly correlated to the one obtained by XRD

Table 2 Elemental analysis

Sample name	Elemental analysis[A]		
	Wt.% S (calculated[a])	Wt.% C (calculated[b])	Wt.% H (calculated[b])
MCM-41	n/m	n/m	n/m
MPS_{HEX}-3%	1.32 (1.56)	7.09 (1.17)	2.43 (0.24)
MPS_{HEX}-6%	2.70 (3.04)	9.10 (2.28)	2.60 (0.47)
MPS_{HEX}-9%	4.04 (4.45)	9.06 (3.33)	2.59 (0.69)
MPS_{HEX}-12%	5.23 (5.79)	11.27 (4.34)	2.97 (0.90)
MPS_{HEX}-15%	6.01 (7.06)	10.48 (5.30)	2.73 (1.10)
MPS_{HEX}-20%	7.88 (9.07)	13.41 (6.80)	3.15 (1.42)
MPS_{HEX}-25%	10.18 (10.92)	14.79 (8.19)	3.41 (1.71)
MPS_{HEX}-30%	12.19 (12.65)	15.39 (9.49)	3.38 (1.98)
MPS_{HEX}-40%	15.06 (15.76)	17.30 (11.82)	3.78 (2.46)
MPS_{HEX}-50%	18.45 (18.50)	17.40 (13.87)	3.93 (2.89)
MCM-48	n/m	n/m	n/m
MPS_{CUB}-3%	1.30 (1.55)	6.77 (1.74)	2.30 (0.34)
MPS_{CUB}-6%	2.56 (3.00)	7.91 (3.37)	2.59 (0.66)
MPS_{CUB}-9%	4.13 (4.36)	9.65 (4.91)	2.69 (0.95)
MPS_{CUB}-12%	5.69 (5.64)	10.66 (6.35)	2.78 (1.23)
MPS_{CUB}-15%	6.93 (6.85)	11.27 (7.71)	2.88 (1.50)
MPS_{CUB}-20%	7.40 (8.72)	12.29 (9.81)	3.00 (1.91)
MPS_{CUB}-25%	8.88 (10.42)	13.40 (11.73)	3.17 (2.28)
MPS_{CUB}-30%	11.48 (11.99)	14.86 (13.48)	3.37 (2.62)
MPS_{CUB}-40%	15.04 (14.75)	16.39 (16.59)	3.59 (3.23)
MPS_{CUB}-50%	17.60 (17.11)	18.76 (19.25)	3.95 (3.74)

n/m = not measured

[A] Errors are 5% for S and 1% for both C and H elements

[a] Calculated following the equation I bellow

[b] Maximum theoretical value

$\%\ S = \frac{100\times 32n}{(R+52)\times n+(100-n)\times 60}$ with R being the molar mass of the organic ligand and n being the % of MPS

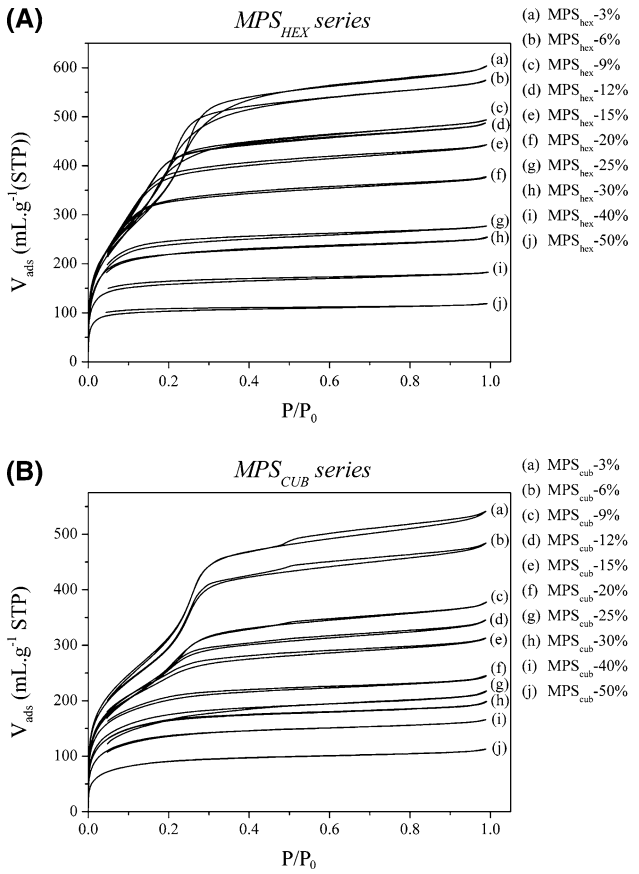

Fig. 5 N_2 adsorption-desorption of (**a**) hexagonal and (**b**) cubic materials

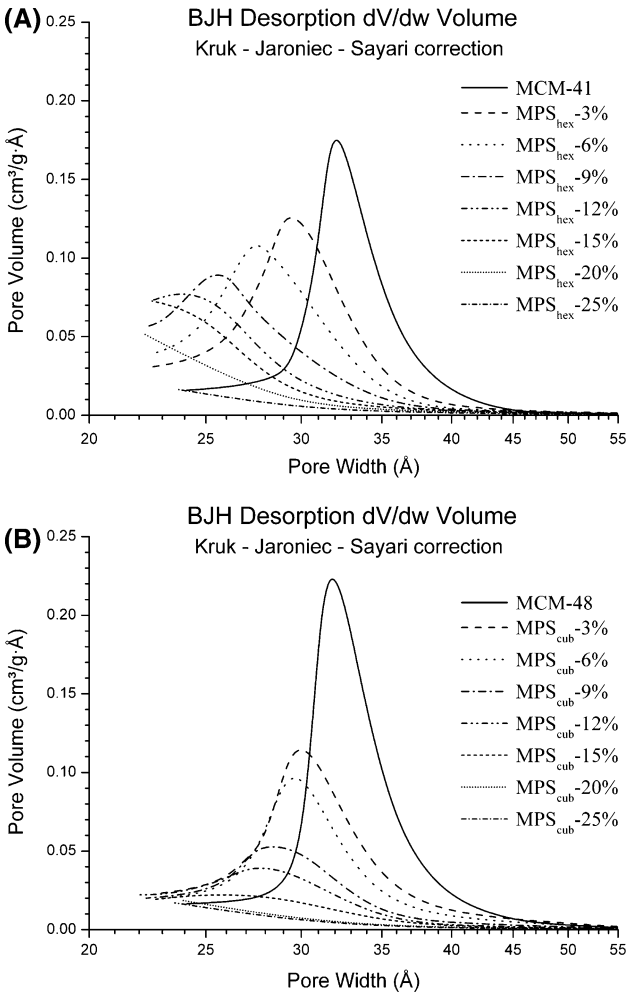

Fig. 6 BJH-KJS study of (**a**) hexagonal and (**b**) cubic materials

measurements and further confirm that for the MCM-41 series, increasing the mercaptopropyl loading will gradually modify the ordered hexagonal porous system to a disordered vermicular network before complete disordering; whereas for the MCM-48 series, the ordered cubic porous network will directly give place to completely disordered materials. Differences can also be noticed by looking at both specific surface area trends. For MPS_{CUB} materials, the specific surface area tends to progressively decrease as the mercaptopropyl loading is increased, whereas for the MPS_{HEX} materials, it increases up to a maxima (in the case of MPS_{HEX}-12%) and then decreases down to a similar value like the one of MPS_{CUB} with a fraction of organosilane equivalent to 40–50%. Finally, only the total pore volume trends in both cases are in some respects similar since this volume decreased in the course of functionalization, only the cubic series diminished faster than the hexagonal series. Again, this latest result is coherent with previous conclusions. From all those results, we found that a 9% mercaptopropyl loading for both cubic and hexagonal systems is the best compromise between enough ligand, an ordered porous framework and an important specific surface area.

3.3 NMR study

3.3.1 ^1H decoupled ^{29}Si MAS NMR spectroscopy

The ^{1}H decoupled ^{29}Si MAS NMR spectra of the MPS_{HEX} and MPS_{CUB} materials are reported in Figs. 9 and 10 respectively. Regardless of the material series and its mercaptopropyl loading, distinct resonances characteristic of siloxane [$Q^n = Si(OSi)_n(OH)_{4-n}$, $n = 2$–4; Q^4 at -110 ppm, Q^3 at -101 ppm, Q^2 at -93 ppm] and organosiloxane [$T^m = RSi–(OSi)m–(OH)3\text{-}m$, $m = 1$–3; T^3 at -65 ppm, T^2 at -56 ppm] species could be observed [87]. Q^4 and Q^3 species were the main components in similar proportions for the low MPS loaded materials regardless of the material geometry, indicating that they were primarily made up of fully condensed silica units with a contribution from incompletely cross-linked units. In addition, the signal-to-noise ratio of these spectra was not very good, we could also detect some Q^2 species only with the relatively low loaded MPS_{CUB} materials (6% to 12%). The presence of

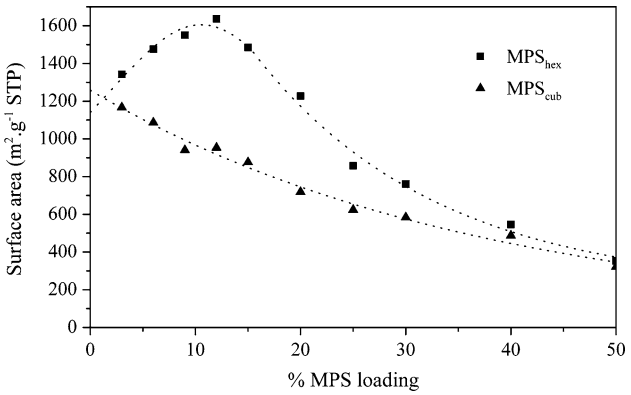

Fig. 7 Specific surface area trends comparison between hexagonal and cubic areas

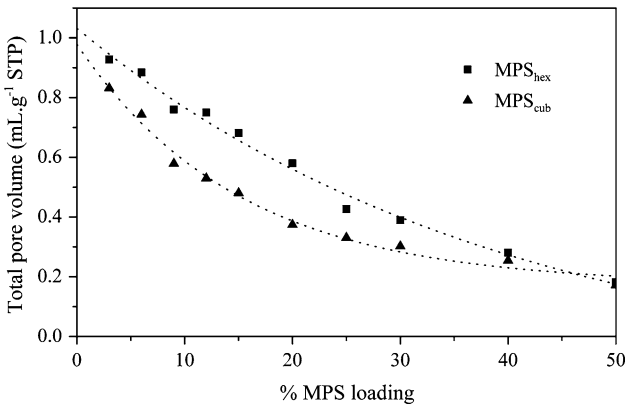

Fig. 8 Total pore volume trends comparison between hexagonal and cubic areas

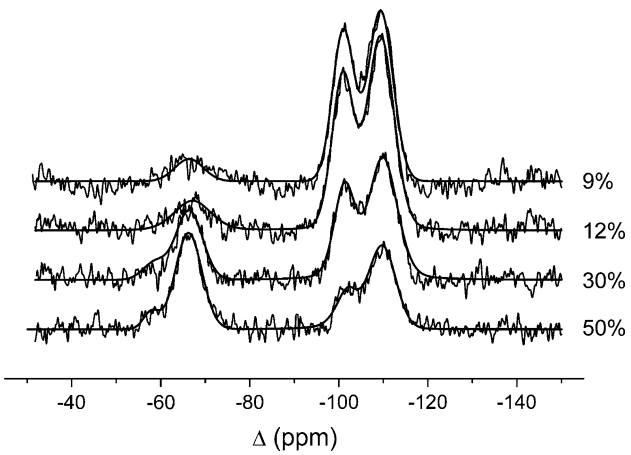

Fig. 9 MPS_{HEX} series -^{1}H DEC ^{29}Si MAS NMR with the deconvolution fit

Si atoms featuring two silanols probably affects more MCM-48 materials due to the closely inter-crossed internal porous framework geometry in addition with the presence of functionalising groups. Resonances characterizing the organosiloxane network (T^3 and T^2) could also be observed

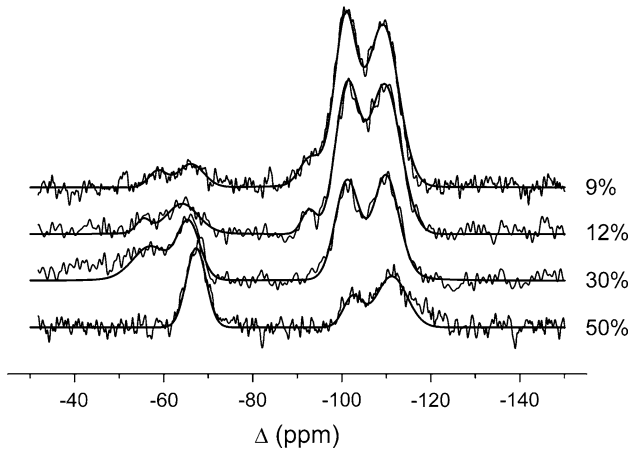

Fig. 10 MPS_{CUB} series -^{1}H DEC ^{29}Si MAS NMR with the deconvolution fit

indicating the presence of MPS moieties inside the silica network. Deconvolution values of the ^{1}H decoupled ^{29}Si MAS NMR spectra (using the WinFit software [88]) giving the relative amounts of Q^n and T^n units are reported in Table 3. As anticipated, the number of T^n units increased linearly with the amount of MPS introduced inside the starting gel confirming the elemental analysis results. The framework condensation degrees (CD) for Q and T species were also calculated. Similarly to previous study, for MPS_{HEX} and MPS_{CUB} samples CD(Q) increased with increasing the MPS functionalization degree [76]. However, CD(T) increased for MPS_{CUB} but decreased for MPS_{HEX} with increasing the MPS functionalization degree.

These results showed that organosiloxanes and silicates species help themselves to condense except in the synthesis media of MSP_{HEX} materials where the condensation of organosiloxanes is hampered. As it is known that, for the in-situ functionalization process, the co-condensation rate is controlled by the experimental conditions [89], it is assumed that the lower amount of water and the nature of the organosilane precursor have influenced reactivity of the organosiloxane species.

3.3.2 ^{13}C CPMAS NMR spectroscopy

The ^{13}C CPMAS NMR spectra of the MPS_{HEX} and MPS_{CUB} materials are reported in Figs. 11 and 12 respectively. From the simulation of ^{13}C NMR spectra by using the ACD-Lab software [90], ^{13}C NMR resonances of the mercaptopropyl group in solution are located in the chemical shift range 8–12 ppm (Si–$\underline{C}H_2$–CH_2–CH_2–SH), 23–27 ppm (Si–CH_2–$\underline{C}H_2$–CH_2–SH), 27–29 ppm (Si–CH_2–CH_2–$\underline{C}H_2$–SH) depending on the condensation degree of the siloxane unit. Consequently, the corresponding solid-state ^{13}C NMR resonances display broad and multi-component line shapes. In both series of

Table 3 ^{1}H decoupled ^{29}Si MAS NMR data[a] for selected MPS materials: corresponding relative peak areas obtained by curve deconvolution and relative peak area ratios

Sample name	Q^4	Q^3	Q^2	T^3	T^2	Q^n	T^n	Q^n/T^n	$\Sigma_n Q^n/4$	$\Sigma_n T^n/3$
MPS_{HEX}-9%	0.52	0.40		0.08		0.92	0.08(0.08)*	11.41	0.89	1.00
MPS_{HEX}-12%	0.54	0.35		0.12		0.88	0.12(0.11)*	7.57	0.90	1.00
MPS_{HEX}-30%	0.47	0.26		0.23	0.05	0.72	0.28(0.29)*	2.63	0.91	0.94
MPS_{HEX}-50%	0.36	0.18		0.42	0.04	0.53	0.47(0.05)*	1.15	0.92	0.95
MPS_{CUB}-9%	0.46	0.40	0.05	0.06	0.03	0.92	0.08(0.09)*	10.83	0.86	0.92
MPS_{CUB}-12%	0.48	0.35	0.04	0.11	0.02	0.87	0.13(0.12)*	6.73	0.88	0.95
MPS_{CUB}-30%	0.38	0.29		0.16	0.17	0.67	0.33(0.29)*	2.06	0.89	0.96
MPS_{CUB}-50%	0.42	0.15		0.42		0.58	0.42(0.51)*	1.36	0.93	1.00

[a] Error for $\%Q^n$ and $\%T^n$ values is about 5%

*T^n values in brackets were calculated from elemental analysis (% S)

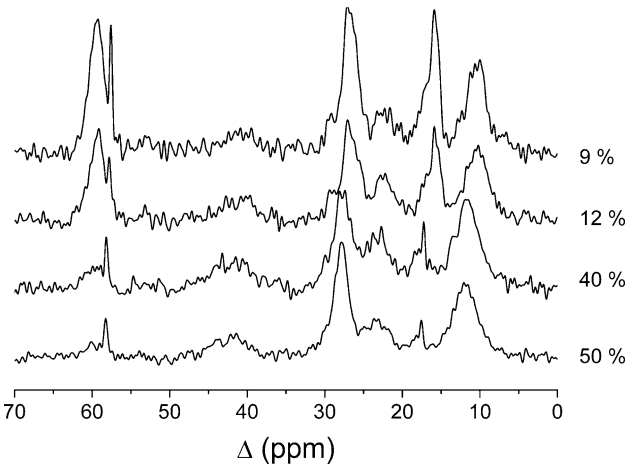

Fig. 11 MPS_{HEX} series -^{13}C CPMAS NMR

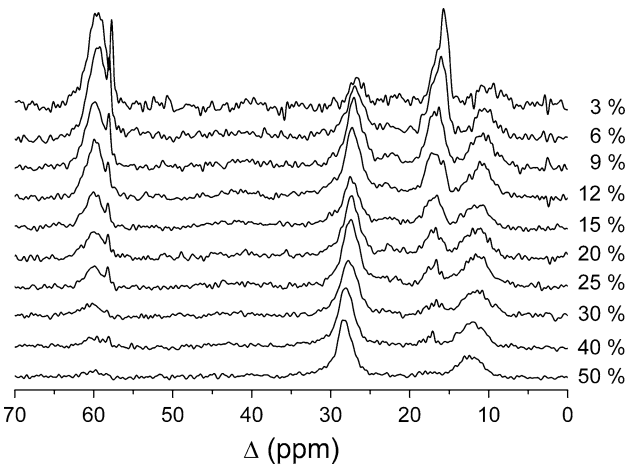

Fig. 12 MPS_{CUB} series -^{13}C CPMAS NMR

materials, the spectra exhibit those broad lines with various intensities depending on the functionalization degree. A shift to low field of resonances characteristic of the propyl chain was also observed with increasing amount of MPS. This phenomenon may be due to the change of conformation of the propyl chain of MPS groups mainly located on the pore surface, which are in a more constraint space when pore size decreases at high MPS loadings. Other lines that cannot be attributed to the mercaptopropyl group are also observable. In the MPS_{CUB} series, there are three extra lines: a broad line centred at 60 ppm with a sharp line at 58 ppm and another broad line centred at 16 ppm with a sharp line at 18 ppm. The broad bands have been assigned to the presence of ethoxy (CH_3–$\underline{C}H_2$–O–Si and $\underline{C}H_3$–CH_2–O–Si, respectively) groups [76]. Previous studies pointed out that these Et–O–Si bounds would form during the surfactant extraction process in the mixture of ethanol/HCl [91]. Therefore, the position of these ^{13}C NMR resonances of the Et–O–Si carbons would depend on the number of accessible reactive Si atoms available inside the porosity. Finally, the sharp lines have been assigned to liquid ethanol (CH_3–$\underline{C}H_2$–OH and $\underline{C}H_3$–CH_2–OH, respectively) present in the porous network probably left during the extraction process. The intensity of these extra lines declines as the fraction of organosilane is increased which is not so much due to the degree of condensation and the functionality of the siloxane *T* or *Q* units [76]; but is probably more a result of the disordering of highly loaded MPS_{CUB} materials since their porosities decrease significantly. These results are to be compared to those obtained by elemental analysis of C and H atoms: clearly, with low loadings of mercaptopropyl precursors, their percentages would be too important if we considered that they come only from the thiol chain and can be explain by the presence of ethoxy chains and ethanol in the materials. Similarly, in the MPS_{HEX} series, the same extra lines are present on the spectra with two additional bands weak in intensities but very broad at ~40 ppm and ~22–23 ppm. The position of those bands excludes the possibility that they may arise from the presence of methanol inside the pore. In addition, the experience showed that methanol or methoxy groups inside a silica framework are almost undetectable by solid-state

NMR, since these molecules are very mobile. After close investigation (especially if any impurity was present in the starting products) and looking to all eventualities, we believe that this couple of bands can be assigned to the presence of the bridged di-sulfide product from two mercaptopropyl silane (i.e.: 3,3,12,12-tetramethoxy-2,13-dioxa-7,8-dithia-3,12-disilatetradecane). Actually, the simulated ^{13}C NMR resonances occur at $\delta = 9$–11 ppm for (–Si–CH_2–CH_2–$\underline{C}H_2$–S)$_2$, $\delta = 21$–26 ppm for (–Si–CH_2–$\underline{C}H_2$–CH_2–S–)$_2$ and $\delta = 38$–40 ppm for (–Si–$\underline{C}H_2$–CH_2–CH_2–S–)$_2$, and fit well with the experimental spectra, since the first band is probably buried in the resonance band of the mercaptopropyl group. The presence of disulfides in the MPS_{HEX} series is probably due to the reaction medium that is more oxidative in presence of methanol [92, 93]. Again, these results totally correlate with those obtained from elemental C and H analyses.

4 Conclusion

MCM-41 and MCM-48 organized mesoporous silica materials of spherical particle shape were successfully functionalized by mercaptopropyl groups by direct functionalization using a co-condensation procedure by varying the mercaptopropyl : TEOS ratio in the synthesis medium. Characterizations of both series of materials have been done and, once again, general categories could be distinguished. However, analyses of the general pore trends revealed important differences between the two series of materials. (1) With low amounts of MPS (up to 9%), the materials had well-ordered mesoporous structures (either hexagonal or cubic mesoporosities) over a rather long range. (2) With slightly more MPS incorporated (between 12% and 20%), each series had a different response: for the MCM-41 series, the materials adopted a mesoporous wormhole structure while reducing the average pore size with increasing mercaptopropyl loading; whether for the MCM-48 series, the materials tended to keep the same structure with a similar pore size with increasing mercaptopropyl loading up to a point (between 20 and 25%) where they became completely disordered. However, for this MCM-48 series it is not excluded that particles are constituted of 2 domains, one ordered with cubic structure and one disordered, which predominates with increase MPS loading. (3) With more MPS ($\geq$25%) incorporated into the materials, both series of materials lost any kind of mesoporous ordering with a monotonic decrease in pore volume with increasing mercaptopropyl loading. With a mercaptopropyl loading higher than 40% both series became almost similar in terms of pore volumes and particle shapes; only ^{13}C and ^{29}Si NMR concluded to differences in the chemical nature of the functionalised silicates mostly due to the nature of the thiol precursor used and the accessibility of reactive Si atoms, but also to the presence of di-sulfide moieties found in the MCM-41 series.

The results of this work could be used in future works as a starting point to study the accessibility to the thiol sites and diffusion rates of the Hg(II) species in the mesoporous solids depending on the sorbent geometry. Such determinations are of importance since not all the active sites located inside the mesoporous structure are accessible [50–55] and the speed at which solution-phase species are allowed to move to these centres is the rate-determining step. The latest point has been highlighted by applications such as electrochemical analysis at chemically modified electrodes [56] or pollutant removal from diluted solutions [29–33]. However, even if some reports have tried to present a qualitative [33] or quantitative [26, 44, 57–65] approach to answer this question of paramount importance; most lacked from direct comparativeness of their results mainly due to the in homogeneity of the materials. Here, we have a batch of materials and their studies of accessibility and diffusion rates could bring the remaining answers.

Acknowledgments This work was supported by the French Ministry of Research and FOMG wish to thanks the French ACI NMAC and the ANR for their financial supports. We are grateful to J. Ghanbaja for taking TEM pictures.

References

1. Yanagisawa T, Shimizu T, Kuroda K, Kato C (1990) Bull Chem Soc Jpn 63:988
2. Kresge CT, Leonowicz ME, Roth WJ, Vartuli JC, Beck JS (1992) Nature 359:710
3. Zhao XS, Lu GQ, Whittaker AJ, Millar GJ, Zhu HY (1997) J Phys Chem B 101:6525
4. Brunel D, Cauvel A, Fajula F, Di Renzo F (1995) Stud Surf Sci Catal 97:173
5. Maschmeyer T, Rey F, Sankar G, Thomas JM (1995) Nature 378:159
6. Burkett SL, Sims GD, Mann S (1996) Chem Commun 1367
7. Macquarrie DJ (1996) Chem Commun 1961
8. Díaz JF, Balkus KJ, Bedioui F, Kurshev V, Kevan L (1997) Chem Mater 9:61
9. Moller K, Bein T (1998) Chem Mater 10:2950
10. Asefa T, MacLachlan MJ, Coombs N, Ozin GA (1999) Nature 402:867
11. Brunel D (1999) Micropor Mesopor Mater 27:329
12. Fryxell GE, Lin Y, Wu H, Kemner KM (2002) Stud Surf Sci Catal 141:583
13. Liu J, Shin Y, Nie Z, Chang JH, Wang L-Q, Fryxell GE, Samuels WD, Exarhos GJ (2000) J Phys Chem B 104:8328
14. Stein A, Melde BJ, Schroden RC (2000) Adv Mater 12:1403
15. Sayari A, Hamoudi S (2001) Chem Mater 13:3151
16. Vinu A, Hossain KZ, Ariga K (2005) J Nanosci Nanotechnol 5:347
17. Lebeau B, Gaslain F, Fernandez-Martin C, Babonneau F (2008) In: Valtchev V, Mintova S, Tsapatsis M (eds) Ordered porous solids, vol 11. Elsevier, p 283

18. Jal PK, Patel S, Mishra BK (2004) Talanta 62:1005
19. Feng X, Fryxell GE, Wang LQ, Kim AY, Liu J, Kemner KM (1997) Science 276:923
20. Mercier L, Pinnavaia TJ (1998) Environ Sci Technol 32:2749
21. Brown J, Richer R, Mercier L (2000) Micropor Mesopor Mater 37:41
22. Liu AM, K Hidajat, S Kawi, DY Zhao (2000) Chem Commun 1145
23. Antochshuk V, Jaroniec M (2002) Chem Commun 258
24. Etienne E, Sayen S, Lebeau B, Walcarius A (2002) Stud Surf Sci Catal 141:615
25. Muñoz A, Rámila A, Pérez-Pariente J, Díaz I, Vallet-Regí M (2003) Chem Mater 15:500
26. Walcarius A, Delacôte C (2005) Anal Chim Acta 547:3
27. Yokoi T, Yoshitake H, Tatsumi T (2004) J Mater Chem 14:951
28. Liu J, Yang J, Yang Q, Wang G, Li Y (2005) Adv Funct Mater 15:129
29. Zhao XS, Lu GQ (1998) J Phys Chem B 102:1556
30. Zemanian TS, Fryxell GE, Liu J, Mattigod S, Franz JA, Nie Z (2001) Langmuir 17:8172
31. Kruk M, Asefa T, Jaroniec M, Ozin GA (2002) J Am Chem Soc 124:6383
32. Beaudet L, Hossain K-Z, Mercier L (2003) Chem Mater 15:327
33. Wei Q, Nie Z, Hao Y, Chen Z, Zou J, Wang W (2005) Mater Lett 59:3611
34. Mercier L, Pinnavaia TJ (1997) Adv Mater 9:500
35. Liu J, Feng X, Fryxell GE, Wang L-Q, Kim AY, Gong M (1998) Adv Mater 10:161
36. Chen X, Feng X, Liu J, Fryxell GE, Gong M (1999) Sep Sci Technol 34:1121
37. Mattigod SV, Feng X, Fryxell GE, Liu J, Gong M (1999) Sep Sci Technol 34:2329
38. Fryxell GE, Liu J, Hauser TA, Nie Z, Ferris KF, Mattigod S, Gong M, Hallen RT (1999) Chem Mater 11:2148
39. Brown J, Mercier L, Pinnavaia TJ (1999) Chem Commun 69
40. Feng X, Rao L, Mohs TR, Xu J, Xia Y, Fryxell GE, Liu J, Raymond KN (1999) Ceramic Trans 93:35
41. Ju YH, Webb OF, Dai S, Lin JS, Barnes CE (2000) Int Eng Chem Res 39:550
42. Fryxell GE, Liu J, Mattigod SV, Wang LQ, Gong M, Hauser TA, Lin Y, Ferris KF, Feng X (2000) Ceramic Trans 107:29
43. Huq R, Mercier L, Kooyman PJ (2001) Chem Mater 13:4512
44. Bibby A, Mercier L (2002) Chem Mater 14:1591
45. Palaniappan Al, Li X, Tay FEH, Li J, Su X (2006) Sens Actuat B 119:220
46. Yiu HHP, Botting CH, Botting NP, Wright PA (2001) Phys Chem Chem Phys 3:2983
47. Goettmann F, Moores A, Boissière C, Le Floch P, Sanchez C (2005) Thin Solid Films 495:280
48. Gao F, Lu Q, Liu X, Yan Y, Zhao DN (2001) Nano Lett 1:743
49. Petkov N, Stock N, Bein T (2005) J Phys Chem B 109:10737
50. Ganesan V, Walcarius A (2004) Langmuir 20:3632
51. Yang LM, Wang YJ, Luo GS, Dai YY (2005) Micropor Mesopor Mater 84:275
52. Walcarius A, Ganesan V (2006) Langmuir 22:469
53. Wang X, Cheng S, Chan JCC (2007) J Phys Chem C 111:2156
54. Marschall R, Bannat I, Caro J, Wark M (2007) Micropor Mesopor Mater 99:190
55. Rac B, Nagy M, Palinko I, Molnar A (2007) Appl Catal A 316:152
56. Hodgkins RP, Garcia-Bennett AE, Wright PA (2005) Micropor Mesopor Mater 79:241
57. Walcarius A (1998) Electroanalysis 10:1217
58. Walcarius A (2001) Electroanalysis 13:701
59. Walcarius A (2001) Chem Mater 13:3351
60. Rabinovich L, Lev O (2001) Electroanalysis 13:265
61. Sayen S, Etienne M, Bessière J, Walcarius A (2002) Electroanalysis 14:1521
62. Walcarius A, Etienne M, Sayen S, Lebeau B (2003) Electroanalysis 15:414
63. Yantasee W, Lin YH, Zemanian TS, Fryxell GE (2003) Analyst 128:467
64. Walcarius A, Delacôte C, Sayen S (2004) Electrochim Acta 49:3775
65. Lesaint C, Frébault F, Delacôte C, Lebeau B, Marichal C, Walcarius A, Patarin J (2005) Stud Surf Sci Catal 156:925
66. Walcarius A, Etienne M, Bessière J (2002) Chem Mater 14:2757
67. Walcarius A, Etienne M, Lebeau B (2003) Chem Mater 15:2161
68. Walcarius A, Delacôte C (2003) Chem Mater 15:4181
69. Etienne M, Lebeau B, Walcarius A (2002) New J Chem 26:384
70. Fontell K, Khan B, Lindstrom KB, Maciejewska D, Puang-Ngern S (1991) Colloid Polym Sci 269:727
71. Vartuli JC, Schmitt KD, Kresge CT, Roth WJ, Leonowicz ME, McCullen SB, Hellring SD, Beck JS, Schlenker JL, Olson DH, Sheppard EW (1994) Chem Mater 6:2317
72. Beck JS, Vartulli JC, Roth WJ, Leonowicz ME, Kresge CT, Schmitt KD, Chu CT-W, Olson DH, Sheppard EW, McCullen SB, Higgins JB, Schlenker JL (1992) J Am Chem Soc 114:10834
73. Moeller K, Kobler J, Bein T (2007) J Mater Chem 17:624
74. Ekwall P, Mandell L, Fontell K (1969) J Colloid Interface Sci 29:639
75. Burkett SL, Sims SD, Mann S (1996) Chem Commun 1367
76. Mori Y, Pinnavaia TJ (2001) Chem Mater 13:2173
77. Lim MH, Stein A (1999) Chem Mater 11:3285
78. Burleigh MC, Markowitz MA, Spector MS, Gaber BP (2001) J Phys Chem B 105:9935
79. Corriu R, Mehdi A, Reyé C, Thieuleux C (2002) Chem Commun 1382
80. Wahab MA, Kim II, Ha C (2004) Micropor Mesopor Mater 69:19
81. Wahab MA, Imae I, Kawakami Y, Ha C-S (2005) Chem Mater 17:2165
82. Melnyk IV, Zub YL, Véron E, Massiot D, Cacciaguerra T, Alonso B (2008) J Mater Chem 18:1368
83. Gregg SJ, Sing KSW (1982) Adsorption, surface area and porosity, 2nd edn. San Diego, Academic Press Inc
84. Everett DH (1972) Pure Appl Chem 31:578
85. Branton PJ, Hall PG, Sing KSW (1993) Chem Commun 1257
86. Branton PJ, Hall PG, Sing KSW, Reichert H, Schüth F, Unger KK (1994) Farraday Trans 90:2965
87. Engelhardt G, Jancke HP (1981) Polym Bull 5:577
88. Massiot D, Fayon F, Capron M, King I, Le Calvé S, Alonso B, Durand J-O, Bujoli B, Gan Z, Hoatson G (2002) Magn Reson Chem 40:70
89. Lesaint C, Lebeau B, Marichal C, Patarin J (2005) Micropor Mesopor Mater 83:76
90. Advanced Chemistry Development, ACD/CHNMR, 1000 (1994–2006)
91. Goletto V, Imperor M, Babonneau F (2001) Stud Surf Sci Catal 135:1129
92. Block E, Aslam M (1988) Tetrahedron 44:281
93. Degl'Innocenti A, Capperucci A (2000) Eur J Org Chem 2171